SIELETERS, an airborne infrared dual-band spectro-imaging system for measurement of scene spectral signatures

Christophe Coudrain, Sylvie Bernhardt, Marcel Caes, Roland Domel, Yann Ferrec, Gouyon Gouyon, Henry Henry, Marc Jacquart, Alain Kattnig, Philippe Perrault, et al.

SIELETERS, an airborne infrared dual-band spectro-imaging system for measurement of scene spectral signatures

Christophe Coudrain,* Sylvie Bernhardt, Marcel Caes, Roland Domel, Yann Ferrec, Rémi Gouyon, Didier Henry, Marc Jacquart, Alain Kattnig, Philippe Perrault, Laurent Poutier, Laurent Rousset-Rouvière, Michel Tauvy, Sophie Thétas and Jérôme Primot

ONERA, The French Aerospace Lab, BP 80100 91123 Palaiseau Cedex, France
**christophe.coudrain@onera.fr*

Abstract: More and more, hyperspectral images are envisaged to improve the aerial reconnaissance capability of airborne systems, both for civilian and military applications. To confirm the hopes put in this new way of imaging a scene, it is necessary to develop airborne systems allowing the measurement of the spectral signatures of objects of interest in real conditions, with high spectral and spatial resolutions. The purpose of this paper is to present the design and the first in-flight results of the dual-band infrared spectro-imaging system called Sieleters. This system has demonstrated simultaneously a ground sampling distance of 0.5m, associated with a spectral resolution of 11 cm^{-1} for the Mid-Wave InfraRed (MWIR) and 5 cm^{-1} for the Long-Wave InfraRed (LWIR).

OCIS codes: (110.0110) Imaging systems; (120.0120) Instrumentation, measurement, and metrology; (110.4234) Multispectral and hyperspectral imaging; (110.3080) Infrared imaging; (120.6200) Spectrometers and spectroscopic instrumentation; (110.4100) Modulation transfer function.

References and links

1. L. Rousset-Rouvière, C. Coudrain, S. Fabre, L. Poutier, T. Løke, A. Fridman, S. Blaaberg, I. Baarstard, T. Skauli, and I. Mocoeur, "SYSIPHE system: a state of the art airborne hyperspectral imaging system. Initial results from the first airborne campaign," Proc. SPIE **9249**, 92490W (2014).
2. Y. Ferrec, J. Taboury, H. Sauer, P. Chavel, P. Fournet, C. Coudrain, J. Deschamps, and J. Primot, "Experimental results from an airborne static Fourier transform imaging spectrometer," Appl. Opt. **50**(30), 5894–5904 (2011).
3. L. Moreau and F. Grandmont, "Review of imaging spectrometers at ABB Bomem," Proc. SPIE **5093**, 82–93 (2003).
4. F. Friedl-Vallon, T. Gulde, F. Hase, A. Kleinert, T. Kulessa, G. Maucher, T. Neubert, F. Olschewski, C. Piesch, P. Preusse, H. Rongen, C. Sartorius, H. Schneider, A. Schönfeld, V. Tan, N. Bayer, J. Blank, R. Dapp, A. Ebersoldt, H. Fischer, F. Graf, T. Guggenmoser, M. Höpfner, M. Kaufmann, E. Kretschmer, T. Latzko, H. Nordmeyer, H. Oelhaf, J. Orphal, M. Riese, G. Schardt, J. Schillings, M. K. Sha, O. Suminska-Ebersoldt, and J. Ungermann, "Instrument concept of the imaging Fourier transform spectrometer GLORIA," Atmos. Meas. Tech. **7**(10), 3565–3577 (2014).
5. www.telops.com/en/hyperspectral-cameras/hyper-cam
6. www.phasicscorp.com
7. B. Fièque, P. Chorier, and B. Terrier, "Sofradir detectors for hyperspectral applications from visible up to VLWIR," Proc. SPIE **7826**, 78261I (2010).
8. H. Hwang, Y. W. Choi, S. Kwak, M. Kim, and W. Park, "MTF assessment of high resolution satellite images using ISO 12233 slanted-edge method," Proc. SPIE **7109**, 710905 (2008).
9. F. Viallefont-Robinet and D. Léger, "Improvement of the edge method for on-orbit MTF measurement," Opt. Express **18**(4), 3531–3545 (2010).
10. C. Miesch, L. Poutier, V. Achard, X. Briottet, X. Lenot, and Y. Boucher, "Direct and Inverse Radiative Transfer Solutions for Visible and Near-Infrared Hyperspectral Imagery," IEEE Trans. Geosci. Rem. Sens. **43**(7), 1552–1562 (2005).
11. W. Marinelli, C. Gittins, B. Cosofret, T. Ustun, and J. Jensen, "Development of the AIRIS-WAD Multispectral Sensor for Airborne Standoff Chemical Agent and Toxic Industrial Chemical Detection," presented at the 2005

#234632 - $15.00 USD Received 13 Feb 2015; revised 7 May 2015; accepted 12 May 2015; published 10 Jun 2015

Parallel Meetings of the MSS Specialty Groups on Passive Sensors; Camouflage, Concealment, and Deception; Detectors; and Materials, Charleston, USA, 14–18 February 2005.
12. W. Johnson, G. Hulley, and S. Hook, "Remote gas plume sensing and imaging with NASA's Hyperspectral Thermal Emission Spectrometer (HyTES)," Proc. SPIE **9101**, 91010V (2014).
13. http://brandywinephotonics.com/wp-content/uploads/2014/05/RELEASE-CHAI-L-320-v4.pdf
14. S. Achal, J.E. McFee, and D. Davison, "Flight and Ground Results from Long-Wave and Mid-wave Airborne Hyperspectral Spectrographic Images," RTO-MP-SET-151 Suffield Defence Research and Development Canada, (2009).
15. T. Jitsufuchi, "Development of a new airborne hyperspectral imager for volcano observations," in *Proceedings of Geoscience and Remote Sensing Symposium (IGARSS)* (IEEE, 2010), pp. 657–660.
16. http://specim.fi/index.php/products/airborne/aisaowl
17. J. Hackwell, D. Warren, R. Bongiovi, S. Hansel, T. Hayhurst, D. Mabry, M. Sivjee, and J. Skinner, "LWIR/MWIR imaging hyperspectral sensor for airborne and ground-based remote sensing," Proc. SPIE **2819**, 102–107 (1996).
18. R. Wright, P. Lucey, S. Crites, K. Horton, M. Wood, and H. Garbeil, "BBM/EM design of the thermal hyperspectral imager: An instrument for remote sensing of earth's surface, atmosphere and ocean, from a microsatellite platform," Acta Astronaut. **87**, 182–192 (2013).
19. K. Yokoyama, H. Miller, Jr., T. Hedman, S. Thordarson, M. Figueroa, J. Shepanski, P. Jarecke, and S. Lai, "NGST longwave hyperspectral imaging spectrometer system characterization and calibration," Proc. SPIE **5159**, 262–274 (2004).
20. P. Lucey, K. Horton, T. Williams, and B. Denevi, "High-performance Sagnac interferometer using uncooled detectors for infrared hyperspectral applications," Proc. SPIE **6565**, 65650S (2007).
21. P. Lucey, M. Wood, S. Crites, and J. Akagi, "A LWIR hyperspectral imager using a Sagnac interferometer and cooled HgCdTe detector array," Proc. SPIE **8390**, 83900Q (2012).
22. J. Hall, R. Boucher, D. Gutierrez, S. Hansel, B. Kasper, E. Keim, N. Moreno, M. Polak, M. Sivjee, D. Tratt, and D. Warren, "First flights of a new airborne thermal infrared imaging spectrometer with high area coverage," Proc. SPIE **8012**, 801203 (2011).
23. M. Ramsey, V. Realmuto, G. Hulley, and S. Hook, "HyspIRI thermal infrared (TIR) band study report," JPL Publ. **12**(16), 1–49 (2012).
24. D. Cabib, "Performance and examples of measurements of a Mid Infrared interferometric hyperspectral imager," Proc. SPIE **7113**, 711310 (2008).
25. P. Lucey, T. Williams, and M. Winter, "Recent results from AHI: a LWIR hyperspectral imager," Proc. SPIE **5159**, 361–369 (2004).
26. H. Miller, K. Shapiro, S. Casement, M. Flannery, and M. Folkman, "Compact, dual band thermal imaging spectrometer for geoscience and remote sensing," in *Proceedings of Geoscience and Remote Sensing Symposium IGARSS* (IEEE, 2012), pp. 2880–2883.
27. P. LeVan and D. Jepson, "3.5-to 12-μm dual-band spectrometer," Opt. Eng. **43**(12), 3045–3054 (2004).

1. Introduction

Hyperspectral imaging systems, combining the evaluation of a scene both in spatial and spectral dimensions, are more and more envisaged to increase the capabilities of airborne system in terms of aerial reconnaissance, for both civilian or military applications. The adjunction of the spectral content of each pixel is said to allow the determination of pollutants in the emanations of a factory, the characterization of the geological content of a region, either to defeat camouflage, and many other applications. However, to confirm the hopes put in this new way of imaging a scene, it is necessary to develop an experimental airborne lab allowing the measurement of spectral signatures of the scenes, in real conditions. The hyperspectral images produced by this airborne lab will be of a great help for the design of future operational systems.

DGA, the French Defence Procurement Agency, entrusted to Onera, the French Aerospace Lab, the development of an airborne hyperspectral imaging system called Sysiphe [1], covering atmospheric bands from the visible to the long wave infrared. The visible, Near InfraRed (NIR) and Short-Wave Infrared (SWIR) part of the system is developed by NEO, Norsk Elektro Optikk in Norway, under contract from the Norwegian defense research establishment (FFI); the infrared part and the processing part are directly developed by Onera. The purpose of this paper is to focus on the infrared dual-band (MWIR and LWIR) spectro-imaging system, called Sieleters, which obtained recently its first in-flight hyperspectral images. In particular, we demonstrate its ability to obtain simultaneously a spectral resolution of 11 cm^{-1} for the MWIR and 5 cm^{-1} for the LWIR, associated to a ground sampling distance

#234632 - $15.00 USD Received 13 Feb 2015; revised 7 May 2015; accepted 12 May 2015; published 10 Jun 2015

of 0.5 m, i.e. an instantaneous field-of-view(IFOV) of 250 µrad, at an altitude of 2000 m (aircraft speed of 73 m. s^{-1}). For the presented results, Sieleters is installed on a DO-228 aircraft, operated by DLR.

This fine spatial resolution is a key element for Sieleters. Indeed, to our knowledge, no operational airborne infrared hyperspectral imager has such an IFOV, as it can be seen on Table 1. This table also emphasizes the low number of current operational MWIR airborne spectral imagers, and that almost half of the instruments listed in this table are (at least partially) cryogenic. Another fact that is worth mentioning is that, except for AIRIS-WAD, all instruments are either slit-based dispersive spectrographs, or Fourier Transform Spectrometers, dynamic or static.

Table 1. Current (2014) MWIR and LWIR airborne spectral imagers

Instrument	company/organism	MWIR	LWIR	IFOV (mrad)	cooled optics	optical concept a
AIRIS-WAD [11]	Physical Sciences Inc. (USA)		x	2.2	[b]	T
HyTES [12]	JPL (USA)		x	1.7	x	D
CHAI L320[c] [13]	Brandywine Optics (USA)		x	1.2	x	D
TASI [14]	Itres (Canada)		x	1.2		D
MASI [14]	Itres (Canada)	x		1.2		D
ARTS [15]	NIED (Japan)		x	1.2		D
AISA-OWL [16]	Specim (Finland)		x	1.1		D
Saris [3]	Bomem (Canada)	x		1		F
SEBASS [17]	The Aerospace Corporation (USA)	x	x	1	x	D
THI [18]	Hawaii Institute of Geophysics and Planetology (USA)		x	1		sF
LWHIS [19]	Northrop Grumman (USA)		x	0.9	x	D
HSI-uncooled [20]	Hawaii Institute of Geophysics and Planetology (USA)		x	0.7		sF
HSI-cooled [21]	Hawaii Institute of Geophysics and Planetology (USA)		x	0.6		sF
Gloria[d] [4]	Karlsruher Institut für Technologie (Germany)		x	0.55	x	F
Mako [22]	The Aerospace Corporation (USA)		x	0.55	x	D
MAGI [23]	The Aerospace Corporation (USA)		x	0.53	x	D
SI-5000[c] [24]	CI Systems (Israel)	x		0.5		sF
AHI [25]	Hawaii Institute of Geophysics and Planetology (USA)		x	0.5	[b]	D
Hypercam LWIR [5]	Telops (Canada)		x	0.35		F
Hypercam MWIR [5]	Telops (Canada)	x		0.35		F
Sieleters B3	Onera (France)		x	0.25	x	sF
Sieleters B2	Onera (France)	x		0.25	x	sF
CDBTIS[c] [26]	Northrop Grumman (USA)	x	x	0.2	x	D
DBIS[c] [27]	AFRL (USA)	x	x	0.073	x	D

[a]T = tunable filter, D = dispersive, F = Fourier transform spectrometer (FTS), sF = static FTS
[b]part of optics is cooled, but not the spectral element (Fabry-Perot for AIRIS and grating for AHI)
[c]to our knowledge, no airborne demonstration, but designed for
[d]limb viewing

In this paper, we will first present the design of the instrument, essentially driven by the simultaneous requirements of measuring the precise spectral signature of each pixel in the scene, with a fine spatial resolution. Then, we will present the first in-flight results, with quantitative evaluations of the global performance.

#234632 - $15.00 USD Received 13 Feb 2015; revised 7 May 2015; accepted 12 May 2015; published 10 Jun 2015

2. Design of Sieleters

To meet the stringent technical requirements, it has been chosen to build Sieleters from two separated imaging spectrometers, each mounted on a stabilization platform. One is dedicated to the MWIR domain and the other one to the LWIR domain. Each instrument works with a specifically designed IR focal plane array, optimized for its spectral domain. This choice was mainly made for two reasons. The first one was to obtain optimized radiometric performances for both MWIR and LWIR instruments (the basic idea is to prevent the strong dark current of the LWIR detector to degrade the signal to noise ratio of the MWIR imaging spectrometer), and the second one was to make the optical design easier.

The design of infrared instruments devoted to applications requiring a high quality in radiometry is essentially governed by the control of the instrumental background. Indeed, the thermal emission of the instrument itself is added to the signature to be measured and can bias its spectral content. Moreover the signal-to-noise ratio is degraded by the quadratic addition of the photon noise related to the instrumental background. So, we have decided to minimize and regulate this parasitic contribution by the realization of a completely cryogenic optical set-up, cooled by liquid nitrogen, for both instruments.

Secondly, the requirement of a precise measurement of the spectral signature from a high speed motion airborne platform, typically moving at a speed of 73 $m.s^{-1}$, leads to a design of a spectro-imaging system with a high efficiency. We therefore decided to develop a high étendue (throughput) infrared imaging Fourier transform spectrometer (IFTS) set-up. Our choice is a static interferometer, similar to a previous system developed in the visible for airborne applications [2]. Indeed, compared to other IFTS [3–5], the static system avoids the use of moving part, which can be very challenging in a cryogenic set-up.

After a brief presentation of the basic principle of static IFTS, next sections will focus on the main components of the system, namely: the optical set-up, with emphasis on the interferometer, the IR focal plane array, and the Line Of Sight (LOS) control. We will also present the main steps of the numerical treatment developed to convert the raw interferograms in hyperspectral images.

2.1 Static IFTS basic principle

Both MWIR and LWIR imaging spectrometers are made of a static Fourier Transform Spectrometer, based on a modified Michelson interferometer, placed in front of the imaging optics. The two arms of the interferometer generate two images of the observed scene in the focal plane of the lens, that match geometrically, but, since the optical path length is different in the two arms, interference fringes are superimposed on the image of the scene.

Then, while the scene is moved perpendicularly to the fringes, by translation of the aircraft at a constant speed, each scene point is successively seen through the set of optical path differences, as illustrated in the next video (Fig. 1).

#234632 - $15.00 USD Received 13 Feb 2015; revised 7 May 2015; accepted 12 May 2015; published 10 Jun 2015

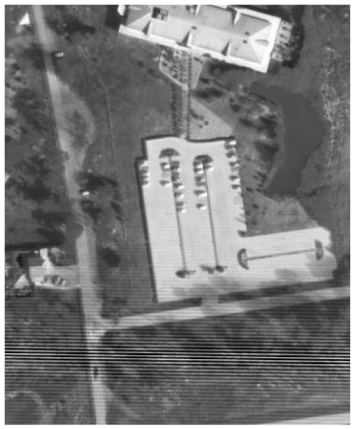

Fig. 1. Imaging principle of IFTS. Each ground element is successively seen through increasing paths differences. (Media 1) is an extract of an acquisition of the MWIR instrument of Sieleters.

2.2 Optical set-up

MWIR and LWIR imaging spectrometers have a similar optical architecture, represented schematically on Fig. 2 below. The two main parts are the Michelson interferometer and the following imaging optics. The light coming from the ground scene first enters into the instrument through a wide-band window, that closes the cryostat in which the optics are integrated. The bending mirror rotates the rays by 90° in order to make them be incident on the beamsplitter inside the interferometer with an angle of 45°. The light then follows its path through the interferometer, propagates into the imaging optics and is finally focused on the optics focal plane. The mirrors of the interferometer are set so that the maximum optical path difference is about 467 µm in the MWIR and 993 µm in the LWIR, to reach the expected spectral resolution.

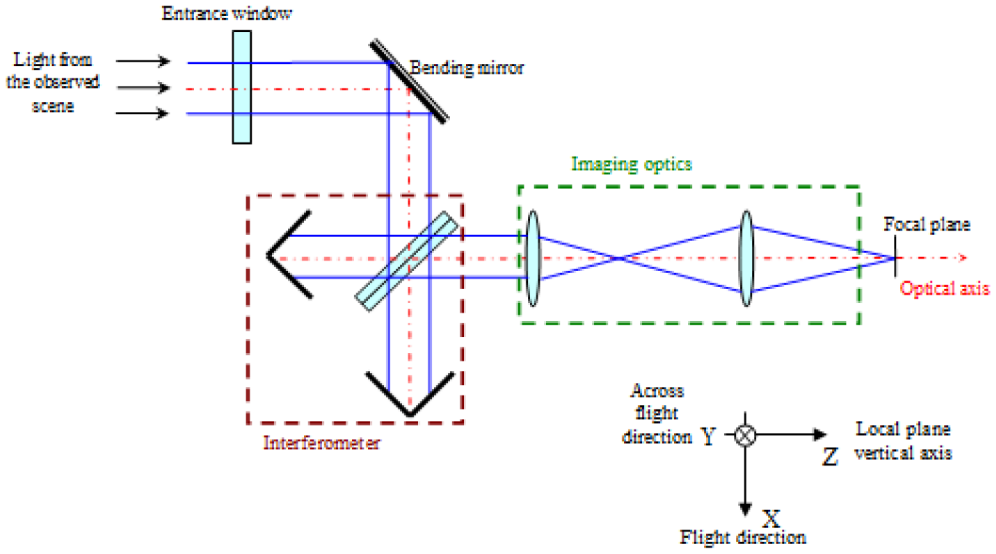

Fig. 2. Optical architecture of the MWIR and LWIR imaging spectrometers.

The mirrors of the Michelson interferometer are dihedrons made of ZnSe plates which are coated with gold. The beamsplitter and compensating plate are also ZnSe plates, which are

#234632 - $15.00 USD Received 13 Feb 2015; revised 7 May 2015; accepted 12 May 2015; published 10 Jun 2015

coated with near perfect separation coating on the splitter side and high transmission anti-reflection coating on the transmittive sides. So, the whole interferometer, including the optical table, is made of ZnSe, which avoids any thermal stress during the cooling. The MWIR and LWIR interferometers were fabricated by Winlight System (see Fig. 3).

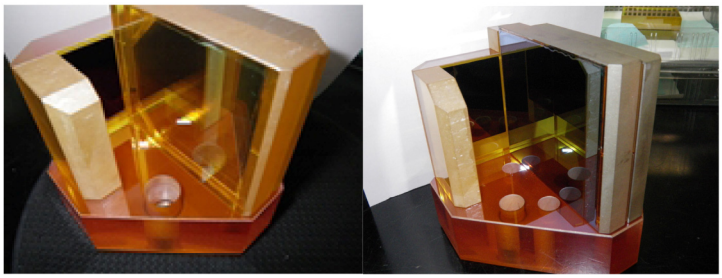

Fig. 3. Interferometric part of Sieleters instruments. Dihedrons, beam splitter, compensating plate and optical table are all made of ZnSe, to avoid any stress during the cooling of the instrument (courtesy of Winlight System).

The imaging lens is entirely made of dioptric elements coated with high transmission anti-reflective coating. The focal length is 100mm for both MWIR and LWIR optics. All the optical components are integrated inside a cryostat, in a vacuum and cryogenic environment (temperature around 100K). The imaging lens is mounted in a tubular mechanical structure embedded into a liquid nitrogen tank. Pressure and temperature sensors are integrated at various locations inside the MWIR and LWIR cryostats in order to verify at each moment that the optics stay in the required environmental conditions. The lens and the opto-mechanical assembly were realized by Winlight System, and the cryogenic assembly with its cryogenic cooling system was manufactured by SDMS. The global performance of the optical part of the two instruments (interferometer and lens), at cryogenic temperature, has been verified with an infrared wavefront sensor (SID4-DWIR [6],), under blackbody illumination. The wavefront aberrations are less than $\lambda/20$ r.m.s., λ being the mean wavelength of the instruments (respectively 4 µm and 10 µm).

2.3 Infrared focal plane arrays

For this specific application, innovative large-format infrared focal plane arrays (IRFPAs) were specifically developed by Sofradir in order to optimize the instrument performances. Both LWIR and MWIR IRFPAs have 1016 × 440 pixels, of 25µm pitch, and the same read-out circuitry [7]. The charge handling capacity of the detectors can be chosen prior to the flight among 4 values (2, 10, 28 or 36Me-) in order to take into account the predicted radiance of the observed scene. Detectors are embedded in a specific cryostat and cooled at a temperature of 77K by a Stirling cryocooler. The requirement of a minimal speed of the aircraft imposes a read-out frequency of 150Hz and implies a very high data rate. Therefore, specific electronic devices have been developed by Onera to drive the IRPFAs and to digitize the high rate and high dynamic data they produce. The amount of data is then transferred into storage units using suitable high rate data link.

2.4 Line of sight control

The control/command of the line of sight (LOS) is a key component of the global instrument. Indeed, it allows both the acquisition of highly resolved individual images and the global ability to precisely superimpose 440 images to obtain the spectral information. As the operating mode of IFTS is unusual, we do not have off-the-shelf industrial stabilized gimbals designed for this mission. So, we decided to develop a specific LOS control system, based on existing industrial products, compatible with an aeronautic Standard camera hole, and to customize them with the support of two companies: Leica Geosystems and Applanix.

#234632 - $15.00 USD Received 13 Feb 2015; revised 7 May 2015; accepted 12 May 2015; published 10 Jun 2015

Moreover, we decided to adopt a specific parallel architecture allowing a direct control of the LOS (closed loop) simultaneously with an a posteriori restitution of the exact LOS by a second independent system (open loop). We also have made the choice to install MWIR and LWIR systems on separate aeronautical certified LOS control systems, in order to offer the opportunity to operate the two bands separately on different types of aircrafts (see Fig. 4).

The closed loop system (CLS) has two main goals. The first one is to correct LOS in real-time, to avoid any filtering in the individual images; it corresponds to a kHz regime and it is classically addressed by off-the-shelf gimbal. The second is to obtain regularly spaced images, ideally translated in the only y-direction; it corresponds to a 1Hz regime. This second regime is specific to the basic principle of static IFTS and requires adaptations, especially in the control laws. CLS is made of:

- A motorized gimbal, based on PAV80 from Leica Geosystem,
- An integrated new generation inertial motion unit based on the µPOS AP from Applanix,
- A mechanical structure allowing a rigid integration of the optical systems of Sieleters, and the tuning of center of gravity, inertial moment and mechanical deformation,
- A control electronic system, based on a DSP (Digital Signal Processing) Microautobox II from dSPACE.

Even if the MWIR and LWIR instruments are completely independent, they give the global impression of a synchronized dance, as can be seen in the next video.

Fig. 4. Sieleters filmed during in-flight data acquisition. The two platforms in red in (Media 2) seem to be mechanically welded, while they are totally independent, in terms of hardware and software.

A good accuracy in the spectral information requires a precise relative positioning of 440 images, with a typical precision of a tenth of the image pitch. So, the real-time closed loop system is completed with an open loop system, allowing the fine post-correction of the instantaneous images. For this reason, an inertial motion unit (IMU) of performance better than 50 µrad on the three axes is installed on each stabilized gimbals. To complete this angular evaluation, the open loop system comprises also a real time DGPS (Differential Global Positioning System). This open loop system allows also the precise projection of the hyperspectral image onto a map, which is a requirement for a large part of the envisaged scientific missions.

#234632 - $15.00 USD Received 13 Feb 2015; revised 7 May 2015; accepted 12 May 2015; published 10 Jun 2015

2.5 Inversion of interferograms

The process to convert raw data to spectral images is very close to the one described in [2]. A non-uniformity correction is first applied to the raw images. Initial guess for offset and gain are estimated at the ground level and are updated, based on the images of the scene themselves, to improve the non-uniformity correction. Images are then registered. This is currently done by image processing (correlation between images), but, at short term, LOS data will be used. Once registered, images are interpolated on a common grid, and spectra are calculated from the interferograms using Fourier inversion, with a phase correction based on previous laboratory measurements. These spectra are radiometrically calibrated also from the laboratory measurements. Spectral images are then georeferenced using LOS data.

3. First in-flight results

The purpose of this section is to present the first results obtained by the two Sieleters instruments during a first flight campaign. The main goal of this campaign was to verify the performances of the payload in terms of spatial and spectral resolutions. It was led in September, 2013, on the French air base of Cazaux, and several sites were overflown in the neighborhood of Cazaux and Toulouse (France).

3.1 LOS performances, closed loop and open loop

The LOS controls systems are realized by integration of an IMU in the closed loop, and the gimbals performances are evaluated by the open loop system which integrates an other IMU (Applanix Postrack 610). Figure 5 shows the residual attitude of the Sieleters LOS during a line acquisition (40 s is the mean time for one line of measurement). The performance of the LOS control must be integrated for one ground pixel. Figure 5 shows this residual error by the standard deviation of each axis integrated on the ground pixel information.

#234632 - $15.00 USD Received 13 Feb 2015; revised 7 May 2015; accepted 12 May 2015; published 10 Jun 2015

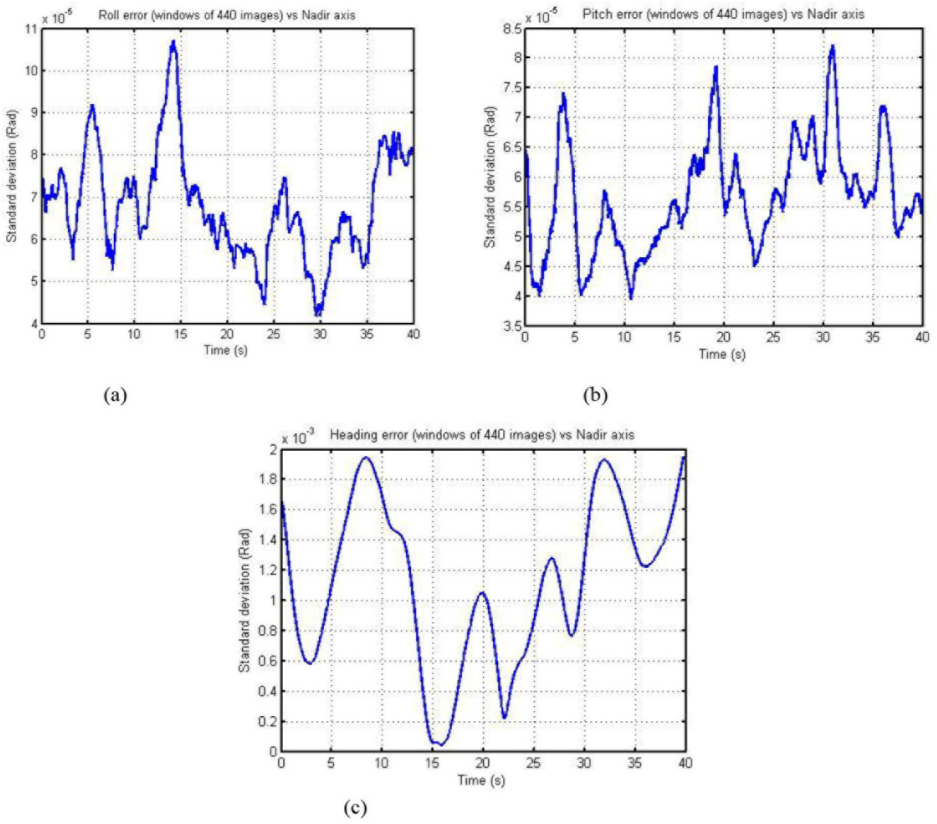

Fig. 5. Evaluation of LOS residual errors obtained from the open loop system: (a) Roll axis, (b) Pitch axis & (c) Heading axis in the reference frame.

From these results, we can deduce that the standard deviation of the LOS is of the order of 80 µrad during the integration time, to be compared with the ifov, equal to 250 µrad.

3.2 Evaluation of the modulation transfer function

As hyperspectral imaging is a new domain, there is no standard Figure Of Merit (FOM), to evaluate the spatial resolution. So, we decided to define a specific FOM, and its associated evaluation procedure. During the flight, all the imaged points of the scene are seen N times, N being the number of lines in the IRFPA. Our choice is to consider the modulation transfer function (MTF) of the reconstructed panchromatic image made of the superposition of all the N lines, after optimal compensation of the aircraft motion and LOS residuals. This panchromatic image is well adapted to MTF evaluation for two main reasons. Firstly, the SNR is very high, ideally $\sqrt{N}$ higher than for an individual image. Secondly, this operation of superposition of all the interference states obtained for one point of the scene implies the disappearance of the fringes issuing from the interferometer, which would potentially disrupt the MTF evaluation.

Practically, MTF is evaluated by the observation of a slanted edge, as it is classically made for in-flight or on orbit optical systems [8]. The site of Cazaux is equipped with a large active infrared target (20 x 20 m^2), allowing the in-flight measurement of radiometric and imaging performances of airborne systems. It is composed with independent panels and is operated in order to obtain a thermal transition of 10 K, between a high temperature homogeneous square of 10 x 10 m^2, inscribed in a low temperature homogeneous square of 20x20 m^2, allowing the

#234632 - $15.00 USD Received 13 Feb 2015; revised 7 May 2015; accepted 12 May 2015; published 10 Jun 2015

observation of two edges in two orthogonal directions. The angle of the slanted edge is tuned by the choice of the aircraft heading.

For our application, the procedure to obtain the MTF from the image of the slanted edge is described in [9]. As we have a precise knowledge of the global filtering of the instrument in lab, we can evaluate the in-flight filtering by multiplying the lab filtering by a model of the transfer function associated to the flight. This model includes the filtering due to the translation of the aircraft during the integration time, which is totally predictable, and the filtering due to the LOS residual error. So, we can simulate an image of the slanted edge with only one degree of freedom: the evaluation of the standard deviation of the LOS residual error. By direct comparison of this image to the recorded image, we can verify the filtering model associated to the flight. Figure 6 shows the simulated target and the measured target. Notice that the south part of the target is not homogeneous, due to a local bad control of the temperature, but it is outside of the useful zone for the MTF evaluation.

(a) (b)

Fig. 6. Basic principle of MTF evaluation. A slanted square image is simulated, from the individual transfer functions measured in the lab and from an evaluation of the additional transfer functions related to the flight. Then, a vertical cut (red dotted line) is extracted for the same relative position in the real (a) and simulated (b) images, for direct comparison (MWIR).

A good fit between model and measurement, as presented in Fig. 7, is obtained for a LOS error standard deviation (Gaussian model) equal to 100 µrad for the two instruments. This value exceeds the restituted value obtained from the open loop (75 µrad, see section 3.1); so, it allows an evaluation of the filtering associated to the post-processing. These values are to be compared with the angular size of the pixel, equal to 250 µrad.

#234632 - $15.00 USD Received 13 Feb 2015; revised 7 May 2015; accepted 12 May 2015; published 10 Jun 2015

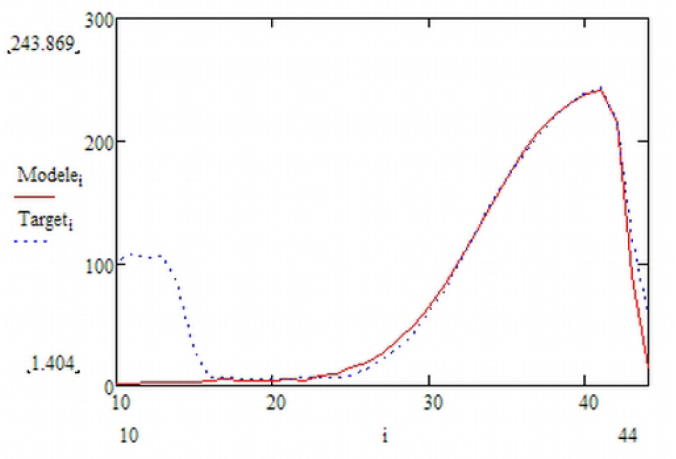

Fig. 7. MTF evaluation by direct comparison between over-sampled edges, respectively extracted from the simulated image (red line) and the actual image (blue dotted line). The difference in the left part of the curve is due to the limited size of the target. X- axis is in pixels ; Y- axis is in arbitrary unit.

With this process, in-flight MTF is evaluated to be respectively higher to 0.14 and 0.09 at Nyquist frequency ($1m^{-1}$) for the MWIR and LWIR instruments (Fig. 8).

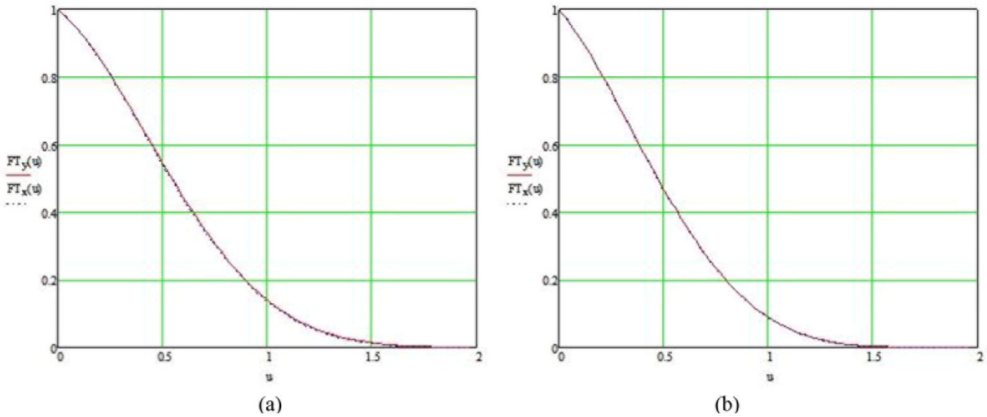

Fig. 8. (a) MTF of the MWIR and (b) the LWIR instruments, for two orthogonal directions x and y. MTF is respectively equal to 0.14 and 0.09 at Nyquist frequency (u = 1, 1m-1).

3 3 Airborne images and spectra

Figure 9 presents an instantaneous interferometric image, obtained at an altitude of 2000 m. Note the horizontal interference fringes (clearly visible near the zero path difference, at the top of the image). The ground footprint is roughly $500x210m^2$, and the ground sampling distance (GSD) is nearly 50 cm. The flight trajectory is vertical (perpendicular to the fringes).

#234632 - $15.00 USD Received 13 Feb 2015; revised 7 May 2015; accepted 12 May 2015; published 10 Jun 2015

Fig. 9. Instantaneous MWIR interferometric image from Sieleters.

From a sequence of 440 images, we obtain an hyperspectral cube. Figure 10 shows an extract of this cube, corresponding to a monochromatic image at 4.8 µm, with a spectral width $\Delta\lambda$ equal to 0.025 µm.

Fig. 10. Monochromatic image (λ = 4.8µm, $\Delta\lambda$ = 0.025µm) from the MWIR hyperspectral cube. The green cross indicates the polystyrene target, and the red cross the concrete area.

Another way to display the information is to consider the spectrum obtained for one point of the scene. So, the spectra of two individual pixels are drawn on Fig. 11. They correspond to a pixel lying inside a large polystyrene target which was set on the ground (green curve), and to a pixel lying on a concrete area (red curve). We also plotted (thin lines on Fig. 11) the expected spectrum for these two ground points. These spectra were obtained by using ground truth simultaneous measurements: the ground spectral emissivity was measured with a SOC400T spectroreflectancemeter, the downwelling irradiance was assessed with a BOMEM MR300 series spectroradiometer pointing at a standard infragold plate and the surface temperature was estimated using 4 KT19 Heitronics LWIR radiometers. The upwelling spectral radiance was then propagated up to the entrance pupil of Sieleters thanks to Comanche propagation model [10]. The atmospheric profile was retrieved from an in situ RPG Hatpro radiometer and the aerosol boundary layer was derived from a CimelCE318 sunphotometer. The quantitative comparison, including an exhaustive error budget, is ongoing.

#234632 - $15.00 USD Received 13 Feb 2015; revised 7 May 2015; accepted 12 May 2015; published 10 Jun 2015

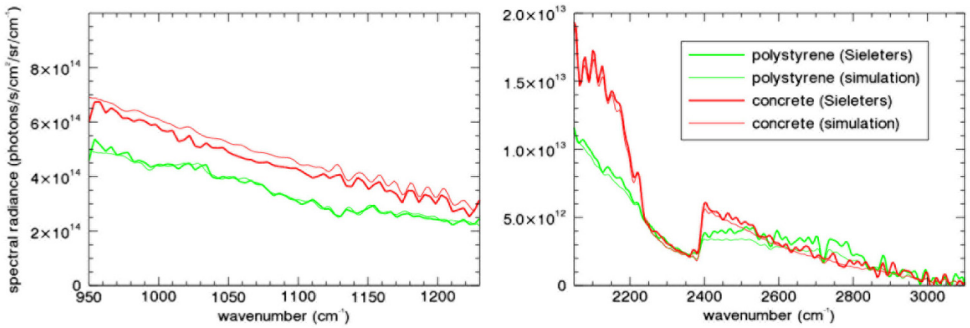

Fig. 11. Spectra of two individual pixels, respectively placed in the polystyrene target (green) and in the concrete target (red), for the LWIR (a) and the MWIR (b). See Fig. 10 for the location of these two pixels. The bold line is for Sieleters measurements, and the thin one for simulated spectra.

4 Conclusion

In this paper, we present the design and the first in-flight results of a new airborne dual-band spectro-imaging system for measurement of scene spectral signatures called Sieleters. This airborne system has demonstrated simultaneously a ground sampling distance of 0.5m, associated to a spectral resolution of 11 cm^{-1} in the MWIR and 5 cm^{-1} in the LWIR. It is in fact composed of two independent sub-systems for MWIR and LWIR, individually certified, to have the opportunity to operate them separately, on different types of aircrafts equipped with a standard camera hole. Image quality has been evaluated by the measurement of the MTF of the panchromatic image, which is higher than 0.09 for both instruments, at Nyquist frequency. We are now going to realize a new campaign for checking the spectral performances. We also work on the establishment of a scientific roadmap and are ready to envisage collaborations for all the domains potentially interested in the infrared hyperspectral imaging: archeology, tracking of the crop, geology or climate change.

Acknowledgments

Sieleters has been developed under DGA funding. The authors want to thank Isabelle Mocoeur from DGA for her interest in this work. They also want to thank C. Lacroix and A. Rousseau from SDMS, D. Soler and E. Tournayre from Winlight System, A. Rohrbach and P. Lemire from Leica Geosystems, J. Ruiz and S. Woolven from Applanix and B. Fièque and P. Chorier from Sofradir, for fruitful discussions.

#234632 - $15.00 USD Received 13 Feb 2015; revised 7 May 2015; accepted 12 May 2015; published 10 Jun 2015